

The iron abundance in hot central stars of planetary nebulae derived from IUE spectra^{*}

J.L. Deetjen, S. Dreizler, T. Rauch, and K. Werner

Institut für Astronomie und Astrophysik, Universität Tübingen, Waldhäuser Strasse 64, D-72076 Tübingen, Germany

Received 11 June 1999 / Accepted 5 July 1999

Abstract. We present the first attempt to determine the iron abundance in hot central stars of planetary nebulae. We perform an analysis with fully metal-line blanketed NLTE model atmospheres for a sample of ten stars ($T_{\text{eff}} \gtrsim 70\,000$ K) for which high-resolution UV spectra are available from the IUE archive. In all cases lines of Fe VI or Fe VII can be identified. As a general trend, the iron abundance appears to be subsolar by 0.5–1 dex, however, the S/N of the IUE spectra is not sufficient to exclude a solar abundance in any specific case. Improved spectroscopy by either FUSE or HST is necessary to verify the possibility of a general iron deficiency in central stars. The suspected deficiency may be the result of gravitational settling in the case of three high-gravity objects. For the other stars with low gravity and high luminosity dust fractionation during the previous AGB phase is a conceivable origin.

Key words: stars: abundances – stars: atmospheres – stars: evolution – stars: AGB and post-AGB – stars: white dwarfs – ultraviolet: stars

1. Introduction

The continuing spectroscopic study of central stars of planetary nebulae (CSPN) is motivated by two observational facts which reveal our incomplete understanding of post-AGB stellar evolution. The first concerns the mere existence of hydrogen-deficient objects which comprise the spectroscopic types [WC] and PG 1159. The second concerns the apparent lack of hydrogen-rich CSPN at the hot end of the white dwarf cooling sequence, suggesting that during this stage all H-rich objects become H-deficient. The first problem initialized an almost complete analysis of all known H-deficient post-AGB stars, resulting in accurate determinations of the effective temperature (T_{eff}) and surface gravity (g), as well as the abundance of the main atmospheric constituents (He, C, O) and in some cases trace of elements (H, N, Ne). The second problem could be solved by the systematic search for (pre-) white dwarf central stars. Sub-

sequent analyses of the H-rich objects revealed T_{eff} , $\log g$, and H:He ratio and the results complement the analyses of other H-rich CSPN performed in numerous previous analyses (see Table 2).

Almost no effort has been yet made to analyze metal abundances in the H-rich CSPN. Interesting insight into AGB evolutionary phases may be gained by such analyses, because obvious abundance anomalies exist among stars with otherwise similar atmospheric parameters (Méndez, 1991). Before embarking on such a project and discussing the abundance patterns it is reasonable to obtain information about the primordial metallicity of these objects by analyzing their iron abundance. The reason herefore is that iron is not affected by nuclear processes during previous evolutionary phases. Such an analysis requires UV spectroscopy. As a first step it is mandatory to check, if the IUE Final Archive contains useful data. It is the aim of this paper to exploit that archive exhaustively in order to identify and analyze quantitatively iron lines in hot central stars.

2. Sample selection and IUE data reduction

Our sample selection started from a CSPN compilation by Méndez (1991) and we complemented his list of H-rich objects with several objects dealt with in the more recent literature (e.g. see Table 2). For these stars we checked the IUE archive for high resolution SWP spectra and found data for 27 H-rich CSPN. From this sample those objects were excluded, which have high mass-loss rates, i.e., those showing Of-type optical spectra and those with extraordinarily strong P Cygni resonance line profiles in the UV. Thereby the final sample consisted of ten stars, which can be analyzed reliably with our static model atmospheres. All program stars have $T_{\text{eff}} \gtrsim 70\,000$ K. Fig. 1 shows their position in the $\log T_{\text{eff}} - \log g$ -diagram and Table 1 summarizes their atmospheric parameters.

The SWP spectra were extracted from the IUE Final Archive and subject to several reduction steps before comparison with model spectra. These steps comprise the assembly of single Echelle orders in order to obtain a complete spectrum in the 1200–1600 Å range; elimination of the strongest interstellar absorption lines by Voigt profile fitting ($\text{Ly}\alpha$ and Si II lines); correction for radial velocity; normalization of the spectra. The last step is rather delicate. Firstly the ripple correction for the Echelle

Send offprint requests to: J.L. Deetjen

^{*} Based on observations with the International Ultraviolet Explorer (IUE) satellite

Correspondence to: deetjen@astro.uni-tuebingen.de

Table 1. The program stars and their atmospheric parameters. Values for T_{eff} [K], $\log g$ [cm s^{-2}], and helium abundance were taken from literature. Columns 5 and 6 list our results for the Fe abundance and the H I column density along the line of sight as derived from the Ly α profile; the references are listed in Table 2

PN	T_{eff}	$\log g$	$n_{\text{He}}/n_{\text{He}\odot}$	$\log n_{\text{Fe}}/n_{\text{Fe}\odot}$	$n_{\text{H I}}$ [cm^{-2}]	references	SWP numbers of co-added spectra
Abell 36	93 000	5.3	1.5	-1.3	$1.9 \cdot 10^{19}$	4, 5, 8, 9	16478, 38132, 47814, 47815
LSE 125	85 000	5.1	0.5	-0.5	$3.0 \cdot 10^{19}$	2, 5	30269
LSS 1362	100 000	5.5	1.0	-0.5	$1.6 \cdot 10^{19}$	3, 4, 5, 8	19830
NGC 1360	110 000	6.0	1.0	-0.5	$3.0 \cdot 10^{18}$	1, 2, 4, 5, 8, 10	55902, 56037, 56038
NGC 1535	70 000	4.6	1.2	-0.5	$1.4 \cdot 10^{19}$	1, 2, 4, 5, 8	56065, 56066
NGC 4361	82 000	5.5	0.5	-1.3	$5.0 \cdot 10^{18}$	1, 2, 4, 5, 8, 9	20440
NGC 6853	99 000	6.8	1.0	-0.5	$3.0 \cdot 10^{18}$	5, 7, 8	18340
NGC 7009	82 000	4.8	0.5	-0.5	$1.5 \cdot 10^{19}$	2, 4, 5, 8	05174, 08580, 08680, 23383
NGC 7293	107 000	7.0	0.5	-0.5	$5.5 \cdot 10^{18}$	4, 9	19859, 48055, 48063
S 216	85 000	6.9	0.1	-0.5	$5.0 \cdot 10^{18}$	4, 6, 7, 8	56071, 56072

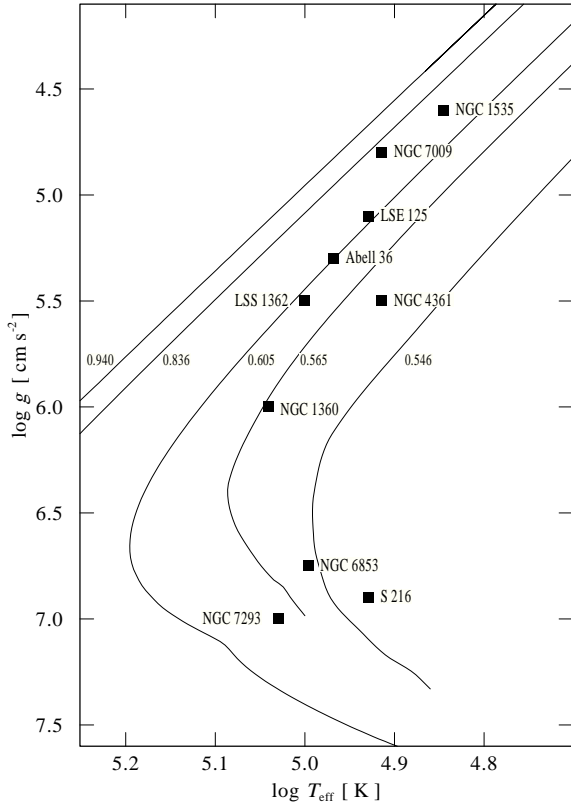


Fig. 1. Location of the program stars in the $\log T_{\text{eff}} - \log g$ diagram compared with post-AGB evolutionary tracks (Schönberner, 1983; Blöcker & Schönberner, 1990) for H-burning stars with different remnant masses (in M_{\odot}) as indicated.

orders in the archival data is far from perfect (see Fig. 2) and has to be corrected. Secondly, fixing the continuum is a rather subjective procedure and thus the major error source for the quantitative analysis, because of the generally high noise level in the spectra. To determine the continuum we smoothed the spectrum with a median filter of 2 Å width, followed by a convolution with a Gaussian profile of 2 Å FWHM. This method is inapplicable in regions with P Cygni profiles and the continuum has to be

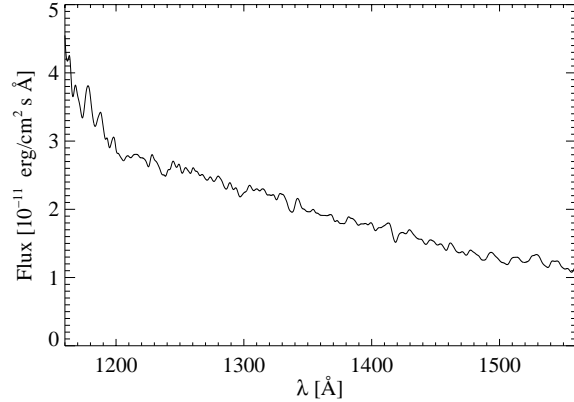


Fig. 2. Calculated continuum of a typical co-added IUE spectrum

Table 2. References in Table 1

1	Méndez et al. (1981)	2	Méndez et al. (1988)
3	Heber et al. (1988)	4	Feibelman & Bruhweiler (1990)
5	Méndez (1991)	6	Tweedy & Napiwotzki (1992)
7	Napiwotzki (1993)	8	Tweedy (1993)
9	Quigley et al. (1993)	10	Hoare et al. (1996)

determined manually. Furthermore the determined continuum around deep ISM lines is too low and has to be raised manually.

3. Model atmospheres

We have calculated a grid of plane-parallel non-LTE model atmospheres (Fig. 3) in radiative and hydrostatic equilibrium. The computer code is based on the Accelerated Lambda Iteration method (Werner & Husfeld, 1985; Werner, 1986) and it can handle the line blanketing of iron group elements by a statistical approach using superlevels and superlines with an opacity sampling technique (Anderson, 1985; Dreizler & Werner, 1993). The latest version of the code and a detailed description of the numerical method can be found in Werner & Dreizler (1999). Our model atmospheres include the CNO elements as well as iron and nickel self-consistently, i.e. their back-reaction on the atmospheric structure is accounted for. In essence, they are very

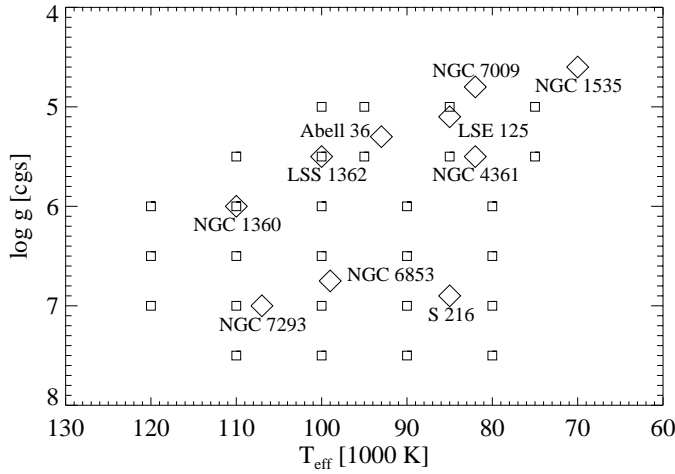


Fig. 3. Distribution of the analyzed CSPN (\diamond) and models (\square) in the $T_{\text{eff}} - \log g$ - plane. For each point of the grid spectra for eight different Fe and Ni abundances have been calculated

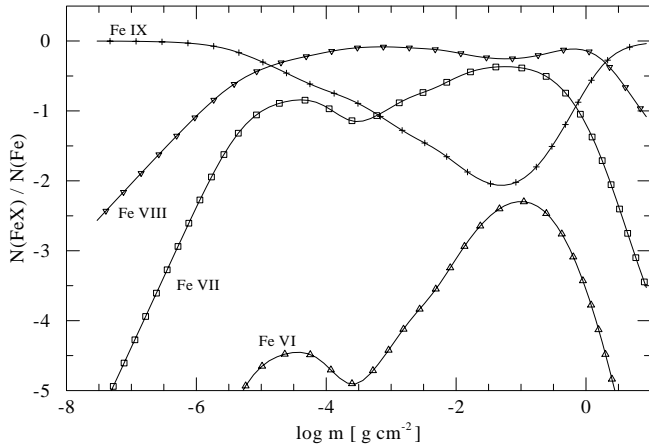


Fig. 4. Ionization structure of iron in a model atmosphere with $T_{\text{eff}} = 110\,000\text{ K}$, $\log g = 6.0$ and solar Fe abundance. Note particularly the relative occupation of Fe VII and Fe VIII in the deeper layers of the atmosphere where the iron lines are formed ($\log m = -2 \dots 0$)

similar to the models described in detail by Haas et al. (1996); Haas (1997), so we restrict ourselves here to a summary of the model atoms in Table 3. The main extension of these models refers to a detailed model atom for Fe VIII. This turned out to be essential in order to reliably compute Fe VII lines, because the relative occupation of both ionization stages sensitively depends on the detailed treatment of their respective level populations via ionization and recombination processes.

As an example, the iron ionization structure in a typical model atmosphere is shown in Fig. 4.

4. Results and discussion

We derived our results with two independent methods. First we compared the observed and theoretical spectra by eye (Fig. 5), second a χ^2 -test has been performed (Fig. 6). To get more reliable results, the χ^2_{red} has been computed only around strong iron lines excluding known ISM lines. As a general trend, the

Table 3. Summary of model atoms used in our model atmosphere calculations. Numbers in brackets denote individual levels and lines used in the statistical NLTE line blanketing approach for iron and nickel. The model atom for each chemical element is closed by a single level representing the highest ionization stage (not listed explicitly)

element	ion	NLTE levels	lines	
H	I	10	36	
He	I	5	3	
	II	10	36	
C	III	6	4	
	IV	4	1	
N	IV	6	4	
	V	4	1	
O	IV	1	0	
	V	6	4	
	VI	4	1	
Fe	IV	7 (6472)	25 (1027793)	
	V	7 (6179)	25 (793718)	
	VI	8 (3137)	33 (340132)	
	VII	9 (1195)	39 (86504)	
	VIII	7 (310)	27 (8724)	
	Ni	IV	7 (5514)	25 (949506)
		V	7 (5960)	22 (1006189)
		VI	7 (9988)	22 (1110584)
VII		7 (6686)	18 (688355)	
	VIII	6 (3600)	20 (553549)	
total		135 (49041)	346 (6565054)	

iron abundance appears to be subsolar by 0.5–1 dex with both methods (see Table 1). However, the S/N of the IUE spectra is not sufficient to exclude a solar abundance in any specific case.

We cannot identify nickel lines for certain, which correspond to an upper limit of a solar nickel abundance. Ni v lines have been detected in other central stars and sdO stars by Schönberner & Drilling (1985), however, these stars have effective temperatures which are lower than those of our objects.

For three high-gravity objects in the sample the suspected iron deficiency may be the result of gravitational settling. For the other stars of the sample with low gravity and high luminosity another explanation must be found since mass loss efficiently suppresses gravitational settling (Ungrlaub & Bues, 1998). Following suggestions in the literature (Lambert et al., 1988; Venn & Lambert, 1990; Bond, 1991; Van Winckel et al., 1992), the iron abundance in these stars might not be primordial, but the result of chemical fractionation through dust formation and subsequent loss due to stellar wind during previous AGB phases.

Therefore improved spectroscopy either by FUSE or HST is necessary to confirm or reject the possibility of a general Fe deficiency in these central stars. Furthermore, the determination of the abundance of CNO-elements is desirable in order to get a better understanding of the chemical evolution of these stars.

Our study suggests that iron is not necessarily a suitable tracer to determine the primordial metallicity. Alternatively one

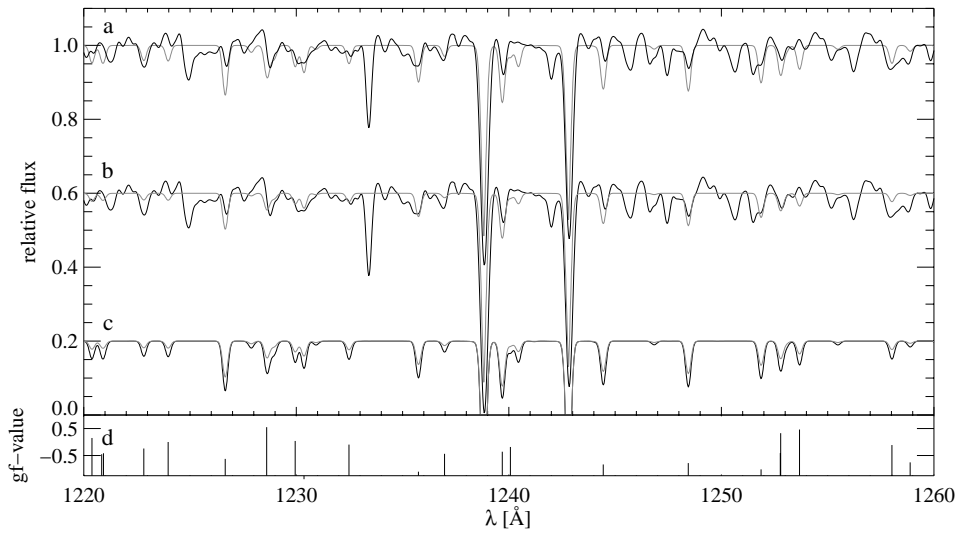
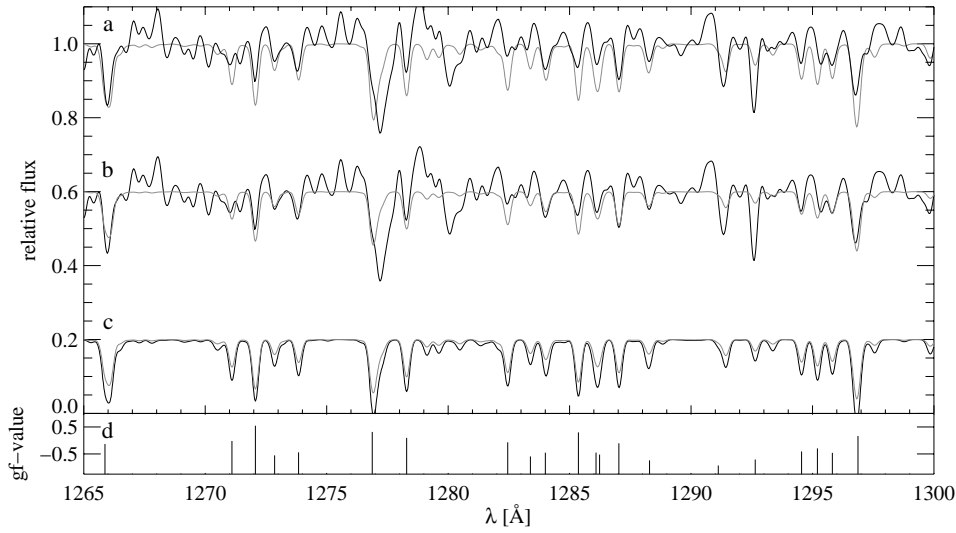


Fig. 5. Details from fits to the iron line spectrum of two central stars. *Top:* S 216; $T_{\text{eff}} = 90\,000\text{ K}$, $\log g = 7.0$; *Bottom:* NGC 1360; $T_{\text{eff}} = 110\,000\text{ K}$, $\log g = 6.0$. Models (dotted): **a** solar Fe and Ni; **b** 0.5 dex subsolar Fe and Ni; **c** comparison of both models; **d** strong Fe VI and Fe VII lines are marked.

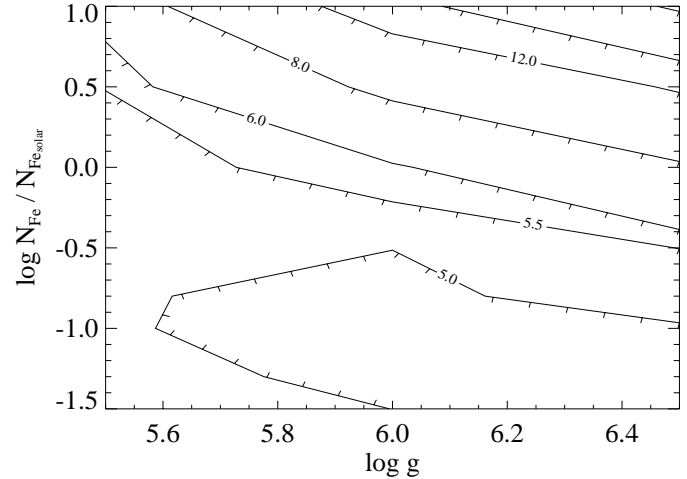
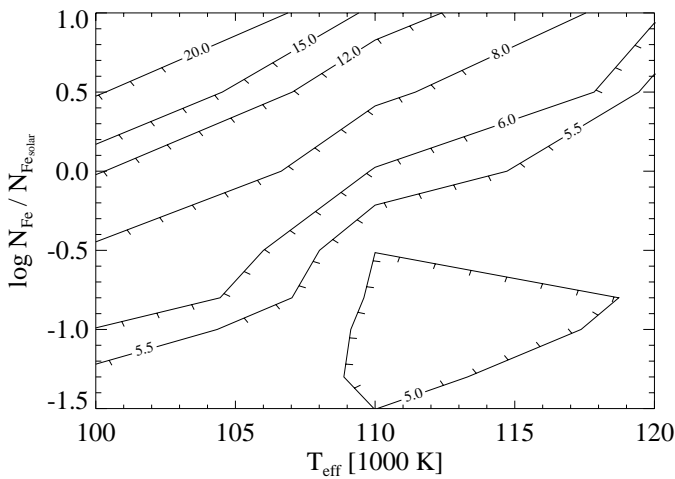


Fig. 6. Contour plot of the χ^2 test for the spectrum of NGC 1360. In the left plot the χ^2_{red} values for those models with $\log g$ at 6.0 and T_{eff} around 110 000 K ($40 = 8 \cdot 5$ models, see Fig. 3) are shown, whereas in the right plot T_{eff} remains fixed and $\log g$ varies. The high χ^2 values (> 5) are due to the low S/N level and the imperfect normalization (see Fig. 2). As a general trend, the χ^2 test favors models with subsolar iron abundance

may use the S or Zn abundance to obtain reliable information (Van Winckel et al., 1992). The abundance of both elements is not affected by nuclear processes during previous evolutionary phases and both elements do not tend to dust formation as iron does (Habing, 1996). Due to the lack of detailed atomic data for Zn, one has to concentrate on the S lines in the FUV and UV region. This emphasizes the need for improved spectroscopic data to solve these questions.

Acknowledgements. We thank S. Haas for helpful discussions and for providing his original version of the iron cross-section sampling software. UV data analysis in Tübingen is supported by the DLR under grants 50 QV 97054 and 50 OR 97055.

References

- Anderson L.S., 1985, ApJ 298, 848
 Blöcker T., Schönberner D., 1990, A&A 240, L11
 Bond H.E., 1991, In: Michaud G., Tutukov A. (eds.) 1991, Evolution of Stars: The Photospheric Abundance Connection. IAU Symp. 145, Kluwer, Dordrecht, p. 341
 Dreizler S., Werner K., 1993, A&A 278, 199
 Feibelman W.A., Bruhweiler F.C., 1990, ApJ 357, 548
 Haas S., 1997, Dissertation, Universität Erlangen-Nürnberg
 Haas S., Dreizler S., Heber U., et al., 1996, A&A 311, 669
 Habing H.J., 1996, A&AR 7, 97
 Heber U., Werner K., Drilling J.S., 1988, A&A 194, 223
 Hoare M.G., Drake J.J., Werner K., Dreizler S., 1996, MNRAS 283, 830
 Lambert D.L., Hinkle K.H., Luck R.E., 1988, ApJ 333, 917
 Méndez R.H., 1991, In: Michaud G., Tutukov A. (eds.) Evolution of Stars: The Photospheric Abundance Connection. IAU Symp. 145, Kluwer, Dordrecht, p. 375
 Méndez R.H., Kudritzki R.P., Gruschinske J., Simon K.P., 1981, A&A 101, 323
 Méndez R.H., Kudritzki R.P., Herrero A., et al., 1988, A&A 190, 113
 Napiwotzki R., 1993, Dissertation, Universität Kiel
 Quigley M.F., Bruhweiler F.C., Feibelman W., 1993, BAAS 25, 1368
 Schönberner D., 1983, ApJ 272, 708
 Schönberner D., Drilling J.S., 1985, ApJ 290, L49
 Tweedy R.W., 1993, MNRAS 260, 855
 Tweedy R.W., Napiwotzki R., 1992, MNRAS 259, 315
 Unglaub K., Bues I., 1998, A&A 338, 75
 Van Winckel H., Mathis J.S., Waelkens C., 1992, Nat 356, 500
 Venn K.A., Lambert D.L., 1990, ApJ 363, 234
 Werner K., 1986, A&A 161, 177
 Werner K., Dreizler S., 1999, The Classical Stellar Atmosphere Problem. In: Riffert H., Werner K. (eds.) Computational Astrophysics. J. Comp. Appl. Math. in press
 Werner K., Husfeld D., 1985, A&A 148, 417